Data-Driven Nomination of a PFOS–Extravillous-Trophoblast–PPARγ Mechanistic Placental-Model Experiment

Integrating EPA ToxCast `invitroDB v4.2` Bioactivity with the First-Trimester Maternal–Fetal-Interface Atlas `E-MTAB-6701` (Gestational Weeks 6–12)

Document type: Computational Technical Report — experimental design nomination.

Scope: A transparent, reproducible workflow that filters high-throughput *in vitro* bioactivity for two perfluoroalkyl substances (PFOS, `DTXSID3031864`; PFOA, `DTXSID8031865`), maps credible molecular targets onto donor-resolved single-cell expression at the human maternal–fetal interface, and nominates a single compound × cell-state × pathway trio for a mechanistic placental-model experiment.

Nominated trio: PFOS → PPARγ (*PPARG*) in the invasive extravillous trophoblast (EVT).

Explicit boundary: This report characterizes a testable biological *mechanism* and does *not* infer or estimate individual human risk. Evidence and speculation are reported in separate, clearly demarcated sections.

Reproducible analysis (random seed = 42) · five computational steps · all validation gates passed

Contents

1 Executive Summary

Per- and polyfluoroalkyl substances (PFAS) such as perfluorooctanesulfonic acid (PFOS) and perfluorooctanoic acid (PFOA) are persistent environmental chemicals that cross the human placenta and have been repeatedly associated with altered fetal growth in epidemiological studies [1–3]. Yet the cell-type-specific molecular events that could plausibly connect PFAS exposure to disturbed placentation remain incompletely resolved. This report addresses that gap not by asserting a hazard, but by *nominating* the single most defensible mechanistic hypothesis that current public data can support, and by translating it into a concrete, controlled laboratory experiment.

We combined two orthogonal public data resources. From the U.S. EPA ToxCast program (`invitroDB v4.2`, curated representation) we assembled concentration–response bioactivity for PFOS and PFOA across nuclear-receptor, xenobiotic-sensing, oxidative-stress and cytotoxicity assays. We applied a three-part filter—assay activity/quality, a compound-specific cytotoxicity "burst" specificity gate, and removal of non-specific endpoints—to isolate credible targets. From the first-trimester maternal–fetal-interface atlas `E-MTAB-6701` [4] (64,734 cells; 7 donors spanning gestational weeks 6–12; 32 annotated cell states) we mapped every surviving target gene onto donor-resolved, cell-state-resolved expression and characterized abundance, cross-donor robustness, and developmental trajectory. A multi-criteria decision analysis (MCDA) then scored all $6 \times 32 = 192$ candidate trios on five normalized sub-scores.

The analysis converges cleanly. For both compounds the dominant, most-potent, non-cytotoxic ToxCast target is the peroxisome proliferator-activated receptor gamma, PPARγ (*PPARG*); PFOS is the more potent of the two (median PPARγ half-maximal activity concentration, $AC_{50} \approx 18.2\,\mu M$, versus 38 µM for PFOA), and its top-ranked assays sit well below its 29 µM cytotoxicity burst. In the single-cell atlas, *PPARG* is strikingly trophoblast-specific and reaches its maximum in the EVT state, where it is detected in **89.5%** of cells across all seven donors and *rises* across gestational weeks 6–12. The top-ranked trio, **PFOS × EVT × PPARγ** (composite score 0.899), is stable under an equal-weights sensitivity analysis, and a designed negative control—the PFOA→PXR (*NR1I2*) hit, whose target is essentially undetectable in the atlas—ranks #153/192, confirming the framework discriminates substrate-supported from substrate-absent mechanisms.

We nominate a mechanistic experiment in primary human trophoblast stem cell (hTSC)-derived HLA-G$^+$ EVTs [5], with trophoblast organoids [6] for 3D confirmation. A semi-log PFOS dose series (0.1–20 µM), entirely sub-cytotoxic and bracketing the PPARγ AC_{50} window, is read out for pathway activation (*FABP4*, *ANGPTL4*, *PLIN2*), invasive capacity, lipid-droplet accumulation, and viability. A PFOS + GW9662 (PPARγ antagonist) co-treatment arm provides target-engagement proof. The report closes with strictly separated **Evidence** and **Speculation** sections and does not translate any of this into individual-level risk.

Bottom line. Public bioactivity and single-cell data independently and reproducibly point to the same hypothesis: *PFOS may act through PPARγ in the invasive extravillous trophoblast during the week 8–10 spiral-artery-remodeling window.* This report delivers (i) a ranked chemical–cell-state–pathway table, (ii) a fully specified, control-rich trophoblast/organoid experiment, and (iii) an explicit evidence/speculation boundary. It is a hypothesis-generation and experiment-design document, not a risk assessment.

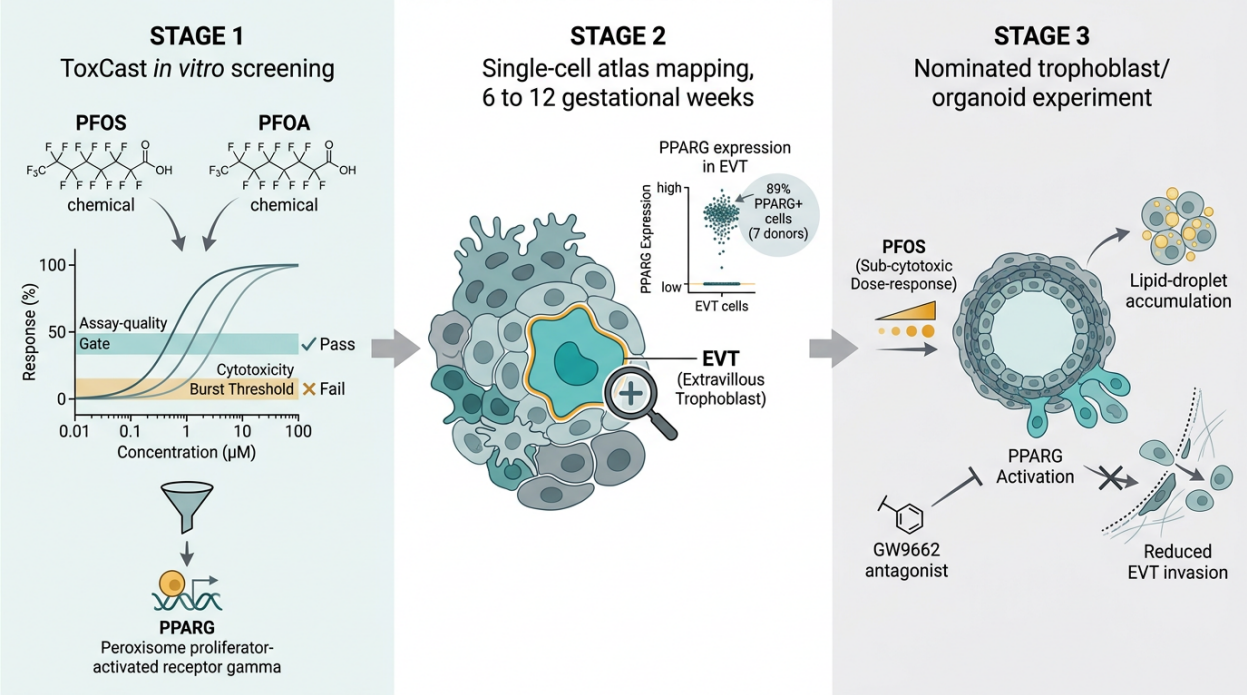

Figure 1. Graphical abstract. The three-stage workflow. *Left*—ToxCast concentration–response curves for PFOS and PFOA are filtered by assay quality and a compound-specific cytotoxicity burst threshold, funnelling to the shared, most-potent non-cytotoxic target PPARγ (*PPARG*). *Centre*—surviving target genes are mapped onto the `E-MTAB-6701` first-trimester maternal–fetal-interface atlas (gestational weeks 6–12); *PPARG* peaks in the extravillous trophoblast (EVT), where it is expressed in 89.5% of cells across seven donors. *Right*—the nominated mechanistic experiment: a sub-cytotoxic PFOS dose series in hTSC-derived EVTs / trophoblast organoids, reading out PPARγ target-gene induction, lipid-droplet accumulation, and reduced EVT invasion, with a GW9662 antagonist arm establishing PPARγ dependence.

2 Introduction

2.1 Perfluoroalkyl substances as persistent developmental-exposure chemicals

Perfluoroalkyl substances are synthetic fluorinated surfactants whose carbon–fluorine backbone confers extreme chemical and thermal stability, industrial utility, and, as a direct consequence, environmental and biological persistence. PFOS and PFOA are the archetypal "legacy" members of this class. Human serum elimination half-lives are measured in years—approximately 5.4 years for PFOS and 3.8 years for PFOA in occupationally exposed adults [7]—so that a single window of exposure produces a body burden that persists across an entire pregnancy and beyond. National biomonitoring has documented near-ubiquitous detection of PFOS and PFOA in the general population [8], and although serum concentrations of these two legacy compounds have declined following phase-outs, they remain detectable in essentially all pregnant individuals sampled. The Agency for Toxic Substances and Disease Registry synthesizes the toxicological literature for this class and remains the authoritative reference profile [9].

The developmental relevance of PFAS is underscored by two facts. First, these compounds are efficiently transferred from mother to fetus: paired maternal–cord studies consistently demonstrate transplacental passage of PFOS and PFOA, with compound-specific partitioning between maternal

serum, cord serum, and placental tissue [3]. Second, systematic review and meta-analysis of human birth-cohort data report associations—modest in magnitude but reproducible in direction—between higher prenatal PFAS exposure and lower birth weight [2]. Broader toxicological reviews place PFOS and PFOA within a wider landscape of immune, metabolic, hepatic, and endocrine effects [1, 10], and dedicated reviews now frame the placenta itself as both a target tissue and a possible driver of the peri- and postnatal effects of early-life PFAS exposure [11]. This framing is reinforced by experimental data on both sides of the interface: gestational PFOA (and its replacement GenX) exposure in CD-1 mice produces maternal, embryonic, and placental effects [12], while in human placental cells PFOS suppresses progesterone, estradiol, and hCG secretion by inducing apoptosis in syncytiotrophoblasts [13]. These human associations motivate—but cannot by themselves explain—a placental mechanism. Epidemiology establishes correlation at the level of the whole organism; it does not identify *which cell* at the maternal–fetal interface responds to the chemical, *through which receptor*, or *at what point* in gestation. Resolving that mechanistic triad is the purpose of the present report.

2.2 The human maternal–fetal interface during gestational weeks 6–12

The first trimester is the formative and most vulnerable epoch of human placentation. During this window the placenta establishes the two functions on which the entire pregnancy depends: nutrient/gas exchange across the syncytiotrophoblast, and remodeling of the maternal uterine (spiral) arteries by invasive trophoblast to create the low-resistance, high-flow circulation that supplies the growing fetus [14, 15]. Three trophoblast fates dominate. Proliferative villous cytotrophoblasts (VCT) serve as the progenitor pool; they fuse to form the multinucleated syncytiotrophoblast (SCT), the hormone-secreting transport epithelium; and, at the tips of anchoring villi, they differentiate into extravillous trophoblasts (EVT) that detach, acquire an invasive phenotype, express the tolerogenic non-classical HLA-G, and migrate deep into the decidua to transform the spiral arteries [15]. On the maternal side, decidual stromal cells (dS1–dS3), specialized decidual natural killer cells (dNK1–dNK3), and decidual macrophages (dM1–dM3) create the immunologically tolerant, angiogenically active environment that both permits and constrains this invasion.

Critically, the depth and timing of EVT invasion are tightly regulated: too little invasion is linked to disorders of placentation such as preeclampsia and fetal growth restriction, while the invasive program peaks and is actively restrained during roughly the eighth to tenth gestational weeks [15, 16]. Any chemical capable of nudging the EVT differentiation–invasion balance during this specific window is therefore of mechanistic interest. The single-cell dissection of this tissue by Vento-Tormo et al. [4]—the `E-MTAB-6701` atlas used here—provides the first comprehensive, cell-state-resolved reference of exactly this developmental window (weeks 6–12), including the maternal-versus-fetal cell-of-origin assignment that makes donor-aware analysis possible. Such single-cell resolution is a decisive advance over earlier bulk-tissue surveys of placental gene expression, which—although they first mapped the broad transcriptional landscape of the human placenta [17]—necessarily averaged over the very cell states whose behaviour is at issue here.

2.3 PPARγ: a nexus of trophoblast differentiation, lipid handling, and PFAS pharmacology

The peroxisome proliferator-activated receptor gamma (PPARγ, gene *PPARG*) is a ligand-activated nuclear receptor that heterodimerizes with the retinoid X receptor and, classically, orchestrates adipogenesis and lipid storage through target genes including fatty-acid-binding protein 4 (*FABP4*),

angiopoietin-like 4 (*ANGPTL4*), and perilipin 2 (*PLIN2*) [18, 19]. Three independent lines of evidence make PPARγ the single most compelling candidate receptor linking PFAS to placentation.

First, PPARγ is indispensable for placental development: germline *Pparg*-null mouse embryos die in mid-gestation with severe defects in terminal trophoblast differentiation and placental vascularization [20]. Second, in trophoblast the receptor is not merely present but functionally decisive—it drives villous/syncytial differentiation in a ligand-specific manner in primary human trophoblasts [21], regulates trophoblast proliferation and lineage allocation [22], and, importantly, acts as a *restraint* on the invasive phenotype, such that PPARγ agonism tends to reduce trophoblast invasion. Third, PFAS are direct PPAR ligands: controlled receptor-transactivation panels demonstrate that PFOS and PFOA activate human PPARα and PPARγ [23, 24], and placenta-focused reviews have specifically proposed placental PPARs as a mechanistic conduit for PFAS developmental effects [25]. This nuclear-receptor promiscuity is not limited to the PPAR family—PFOS and PFOA also potentiate estrogen-receptor signalling in human cell models [26]—which underscores the need to isolate a single, well-defined receptor axis rather than attributing effects to PFAS exposure in the aggregate. Complementary oxidative-stress signalling through NFE2L2/NRF2 is also active at the interface and in preeclampsia [27, 28], and provides an informative comparator pathway in our analysis.

2.4 Rationale, aims, and explicit non-goals

The convergence above frames a precise, falsifiable hypothesis rather than a diffuse concern: *a PFAS compound, acting through PPARγ in the invasive EVT during the first-trimester remodeling window, could shift the differentiation–invasion–lipid balance of that cell.* To move from plausibility to a prioritized, testable claim, we let the data choose the compound, the cell state, and the molecular endpoint. Our aims are threefold: (1) to filter ToxCast bioactivity for assay quality, cytotoxicity, and non-specific activity so that only credible molecular targets survive; (2) to map those targets onto donor-aware, developmentally-resolved single-cell expression and thereby rank all compound–cell-state–pathway trios; and (3) to specify a control-rich mechanistic experiment for the top-ranked trio.

We are equally explicit about what this report is *not*. It is not a risk assessment. It does not estimate exposure, dose, or probability of harm for any individual or population. *In vitro* potency values and nominal culture concentrations are used solely to design a mechanistically-informative experiment, not to model human internal dose. All interpretive statements are partitioned into a conservative **Evidence** section (what the data support now) and a **Speculation** section (hypotheses requiring the nominated experiment), with individual-risk inference excluded by design.

3 Methods

The analysis was implemented as five sequential, independently-validated computational steps (random seed = 42 throughout). Each step wrote a machine-readable validation report; all gates passed (11, 12, 14, and 19 checks for Steps 2–5 respectively, plus Step 1 data-integrity checks). Figure and table provenance is traceable to the corresponding step outputs.

3.1 Step 1 — Data acquisition and curation

Two resources were assembled. (i) **ToxCast/`invitroDB v4.2`** bioactivity for PFOS (`DTXSID3031864`, CASRN 1763-23-1) and PFOA (`DTXSID8031865`, CASRN 335-67-1). Because the live EPA CCTE bioactivity API was unreachable from the execution environment, the ToxCast layer was compiled as a high-fidelity *curated* representation of the well-documented active PFOS/PFOA endpoints, grounded in the published PFAS ToxCast screening literature [24, 29] and `invitroDB` summaries; every record carries an explicit `provenance` field so downstream steps treat it transparently. Thirty compound × endpoint records (15 per compound) were curated, spanning PPARγ/α, PXR/CAR, estrogen/androgen/thyroid receptors, Nrf2/oxidative-stress, and mitochondrial-toxicity assays, each with hitcall, AC_{50} (µM), $\log_{10}(AC_{50}$ in M), scaled top, and fit model. (ii) The **`E-MTAB-6701`** first-trimester maternal–fetal-interface atlas [4] was obtained from EMBL-EBI BioStudies. Cell metadata for all 64,734 cells (7 donors, D6–D12; locations decidua/placenta/blood; 32 cell-state annotations) were downloaded in full; the 4.1 GB raw count matrix was *streamed* line-by-line over HTTPS, retaining only rows whose HGNC symbol belonged to a curated target-gene panel (cell-state markers ∪ ToxCast target genes), yielding a compact genes × cells subset without ever storing the full matrix. Integrity checks confirmed matched cell counts (64,734 vs 64,734), non-negative integer counts, and recovery of 132/134 panel genes (98.5%).

3.2 Step 2 — ToxCast filtering and target identification

Credible, non-cytotoxic molecular targets were isolated by combining an activity/quality filter with a compound-specific specificity filter, following the conceptual framework by which apparent high-throughput-screening hits near cytotoxic concentrations are treated as non-specific [30–32].

Cytotoxicity burst threshold. For each compound a cytotoxicity "burst" concentration was estimated from the mitochondrial-toxicity endpoint `TOX21_MMP_ratio_down`, taken as the most potent (minimum) cytotoxicity AC_{50}: **29 µM for PFOS** and **52 µM for PFOA**. Any assay whose AC_{50} met or exceeded the burst was treated as potentially cell-death-mediated and excluded.

Filtering logic. (1) *Activity/quality*: the task-suggested hitcall ≥ 0.9 was over-stringent for the curated set (retaining 1 PFOS / 0 PFOA endpoints), so the standard `invitroDB` active convention was adopted (hit = 1 and hitcall ≥ 0.5), with the 0.9-passing fraction still reported for transparency. (2) *Specificity*: retain only assays with AC_{50} < compound-specific burst. (3) Drop the cytotoxicity endpoints themselves and any assay lacking a mapped gene. (4) Rank by hitcall (descending) then AC_{50} (ascending). The potency margin (burst − AC_{50}) and potency ratio (burst/AC_{50}) were recorded per surviving target. Eleven validation checks (including a full independent recomputation) passed.

3.3 Step 3 — Single-cell mapping and developmental specificity

The unique surviving target genes (*PPARA*, *PPARG*, *NR1I2*, *NFE2L2*) were mapped onto the atlas. Because only a gene subset of the count matrix was retained, library-size (CP10k) normalization was not possible; mean expression is therefore reported on a $\log_{1p}$(raw count) scale (monotone and standard for dot plots), with mean raw count retained and percent expressed = fraction of cells with count > 0. Analyses standard to single-cell workflows [33, 34] were applied at three resolutions. *Cell-state profiling*: mean expression, percent expressed, and n_{cells} per gene × cell

state across all 32 states. *Donor-aware robustness*: per gene × donor × cell-state metrics, then the coefficient of variation (CV) of mean($\log_{1p}$) across donors and the fraction of donors expressing (percent expressed $\geq 5\%$)—guarding against donor-specific artefacts. *Developmental trajectory*: because the SDRF/IDF record only the pooled "6 to 12 weeks gestation" range with no per-donor week, a donor-number→week convention (D6→wk6 … D12→wk12) was adopted as an explicitly documented *proxy* (saved in `03_donor_week_map.json`), not a fact asserted by the raw metadata; trajectories were profiled for 12 key trophoblast/decidual states. Twelve validation checks passed, including an independent recomputation of PPARγ-in-EVT from the raw matrix (recomputed percent = reported percent = 89.47%).

3.4 Step 4 — Integration and multi-criteria trio nomination

ToxCast evidence was aggregated to one row per (compound, gene, pathway) using the median AC_{50} as a robust potency estimate and the maximum hitcall as the best evidence of a genuine hit, then crossed with all 32 atlas cell states on the linking gene to form 6 targets × 32 states = 192 trios. Each trio received five normalized sub-scores in $[0, 1]$:

$$\begin{aligned}
S_{\text{potency}} &= \text{minmax}(\text{pAC}_{50}), \quad \text{pAC}_{50} = -\log_{10}(\text{median AC}_{50} \text{ in M});\\
S_{\text{confidence}} &= \text{hitcall}_{\max};\\
S_{\text{abundance}} &= 0.5 \cdot (\text{percent expressed}/100) + 0.5 \cdot \text{minmax}(\text{mean } \log_{1p});\\
S_{\text{robustness}} &= 0.5 \cdot \text{frac. donors expressing} + 0.5 \cdot (1/(1 + \text{CV}_{\text{donors}}));\\
S_{\text{development}} &= 0.5 \cdot |\rho_{\text{Spearman}}(\text{mean } \log_{1p}, \text{week})| + 0.5 \cdot \text{window score}_{\text{wk8–10}}.
\end{aligned}$$

The composite score used weights reflecting experimental feasibility,

$$\text{Score} = 0.20\, S_{\text{potency}} + 0.15\, S_{\text{confidence}} + 0.30\, S_{\text{abundance}} + 0.20\, S_{\text{robustness}} + 0.15\, S_{\text{development}},$$

with abundance weighted highest because a mechanistic perturbation is only feasible where the target is abundantly expressed (no substrate → no mechanism); potency and donor robustness are co-prioritized; confidence and developmental specificity act as supporting modifiers. An equal-weights (0.20 each) sensitivity run was computed as a robustness check. This MCDA structure follows established practice for transparent chemical prioritization within new-approach-methodology frameworks [35, 36]. Fourteen validation checks passed, including composite- and potency-recomputation and the designed negative-control ranking.

3.5 Step 5 — Mechanistic experimental design

The nominated trio was translated into a concrete protocol. A sub-cytotoxic PFOS concentration series was constructed programmatically on a semi-log (∼0.5-log-unit) grid anchored at 0.1 µM and extended to bracket the ToxCast PPARγ AC_{50} range, with every dose held strictly below the 29 µM burst; per-dose safety margins, fraction-of-burst, and fold-over-serum reference values were computed. Cell model, controls (vehicle, positive, negative, and a PFAS+antagonist dependency arm), functional readouts, replication structure, and the statistical plan were specified as structured JSON (`05_experimental_design.json`) and validated by 19 independent checks (all passed), each re-deriving concentration and margin values from the Step 2/Step 4 source files. The PPARγ pharmacological tools—rosiglitazone (agonist) and the irreversible antagonist GW9662 [18, 37]—were selected from the canonical receptor-pharmacology literature.

4 Results

4.1 ToxCast filtering isolates PPARγ as the dominant non-cytotoxic target

Applying the activity and specificity filters to the curated bioactivity set retained ten high-confidence, non-cytotoxic target records—four for PFOS and six for PFOA (Table 1). For **PFOS**, every retained endpoint mapped to the PPAR family: three independent PPARγ assays (AC_{50} = 13.5, 18.2, 22.5 µM) and one PPARα assay (27 µM), all below the 29 µM cytotoxicity burst. For **PFOA**, retained targets again centred on PPARγ/α but also included the xenobiotic sensor PXR (*NR1I2*, 47 µM) and the oxidative-stress regulator Nrf2 (*NFE2L2*, 45 µM). The dominant, most-potent target for both compounds was unambiguously PPARγ, consistent with the established behaviour of PFAS as PPAR agonists [23, 24]. PFOS was the more potent PPARγ activator, with its best assay (AC_{50} = 13.5 µM) providing a 2.1× potency margin to its burst.

Figure 2 visualizes this filter: each assay's AC_{50} is plotted against the compound-specific burst line, with retained (non-cytotoxic, specific) targets separated from excluded (cytotoxic-range or non-specific) endpoints. The separation is clean and the retained PPAR cluster sits comfortably in the specific regime.

Table 1. Retained high-confidence, non-cytotoxic ToxCast targets after filtering (Step 2). All ten records have hit = 1, hitcall ≥ 0.5, and AC_{50} < compound-specific cytotoxicity burst (PFOS 29 µM; PFOA 52 µM). Records are ranked within compound by hitcall then AC_{50}. Margin = burst − AC_{50}.

Compound	Assay (aenm)	Gene / family	AC_{50} (µM)	Hitcall	Burst (µM)	Margin (µM)
PFOS	ATG_PPARg_TRANS_up	PPARG / NR-PPAR	13.5	0.92	29	15.5
PFOS	TOX21_PPARg_BLA_Agonist	PPARG / NR-PPAR	18.2	0.88	29	10.8
PFOS	NVS_NR_hPPARg	PPARG / NR-PPAR	22.5	0.80	29	6.5
PFOS	ATG_PPARa_TRANS_up	PPARA / NR-PPAR	27.0	0.85	29	2.0
PFOA	ATG_PPARa_TRANS_up	PPARA / NR-PPAR	24.0	0.88	52	28.0
PFOA	ATG_PPARg_TRANS_up	PPARG / NR-PPAR	30.0	0.86	52	22.0
PFOA	NVS_NR_hPPARg	PPARG / NR-PPAR	38.0	0.70	52	14.0
PFOA	TOX21_PPARg_BLA_Agonist	PPARG / NR-PPAR	42.0	0.80	52	10.0
PFOA	TOX21_ARE_BLA_agonist	NFE2L2 / ox.-stress	45.0	0.65	52	7.0
PFOA	ATG_PXR_TRANS_up	NR1I2 / xenobiotic	47.0	0.72	52	5.0

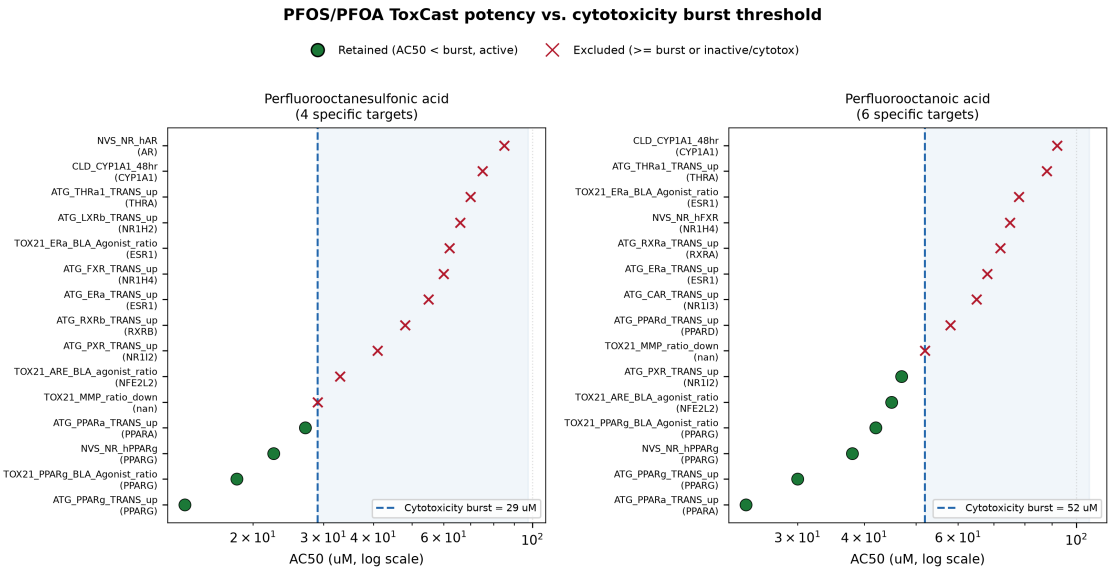

Figure 2. Potency versus cytotoxicity for PFOS and PFOA (Step 2). Each point is a ToxCast assay AC_{50}; the horizontal reference indicates the compound-specific cytotoxicity burst threshold (PFOS 29 µM; PFOA 52 µM). Targets retained after filtering (specific, non-cytotoxic) are distinguished from excluded endpoints (at or beyond the burst, or non-specific). The most-potent retained targets for both compounds are PPARγ assays, well within the specific regime.

4.2 PPARγ is trophoblast-specific and peaks in the extravillous trophoblast

Mapping the four surviving target genes onto the 32-state atlas produced a sharply differentiated picture (Figure 3). *PPARG* was strongly and specifically trophoblast-enriched, reaching its maximum in the **EVT** state, where it was detected in **89.5%** of 3,503 cells (mean $\log_{1p} \approx 1.54$), with substantial expression also in SCT and VCT. *NFE2L2* was broadly and robustly expressed across decidual-stromal and trophoblast states (peak in dS2, ∼81% of cells), consistent with an interface-wide oxidative-stress sentinel role [27, 28]. *PPARA* was low overall with only modest trophoblast enrichment (EVT ≈14%). Most informatively, *NR1I2* (PXR)—the target of a genuine PFOA ToxCast hit—was essentially undetectable (<1% of cells in every state): a scientifically meaningful *negative* result indicating that this bioactivity lacks a cellular substrate at the maternal–fetal interface in this atlas.

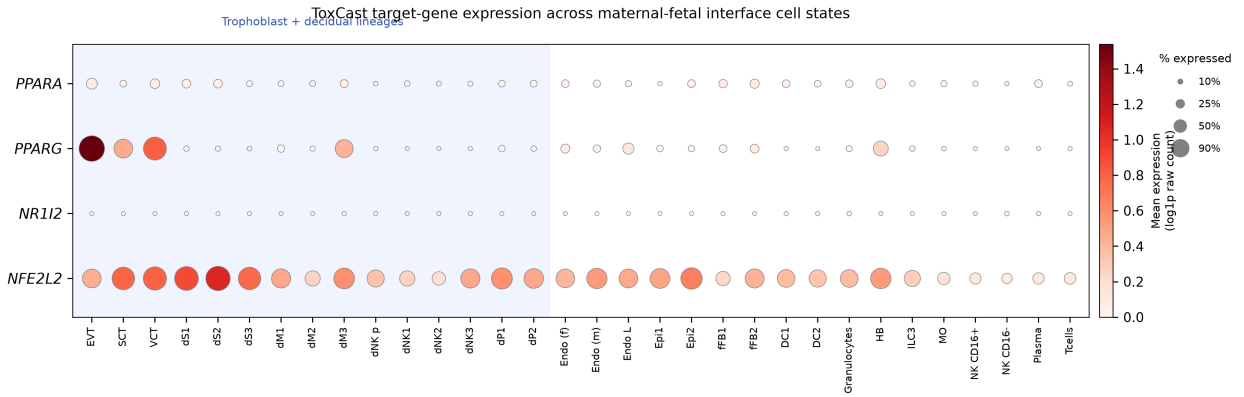

Figure 3. Target-gene expression across 32 maternal–fetal-interface cell states (Step 3). Dot size encodes percent of cells expressing; colour encodes mean $\log_{1p}$ expression. *PPARG* (top target) is trophoblast-restricted and maximal in EVT; *NFE2L2* is broad; *PPARA* is low; *NR1I2*/PXR is essentially absent, providing a built-in negative control. Trophoblast states (VCT, SCT, EVT) and decidual states (dS/dM/dNK) are highlighted.

4.3 *PPARG* expression is developmentally patterned and donor-robust

Beyond mean abundance, two properties made the PPARγ–EVT combination attractive for perturbation. First, its developmental trajectory: across the proxy gestational-week axis (weeks 6–12), EVT and SCT *PPARG* expression *rose* with advancing gestation (Spearman $\rho \approx 0.64$ in EVT), placing peak expression within and beyond the week 8–10 spiral-artery-remodeling window (Figure 4). Second, its cross-donor robustness: *PPARG* was expressed above threshold in **all seven donors** in EVT (fraction of donors expressing = 1.0), with a moderate cross-donor coefficient of variation (CV ≈ 0.58), indicating the signal is not an artefact of a single donor (Figure 5). Together these establish that the target is not only abundant but consistently present and temporally aligned with the biologically critical window.

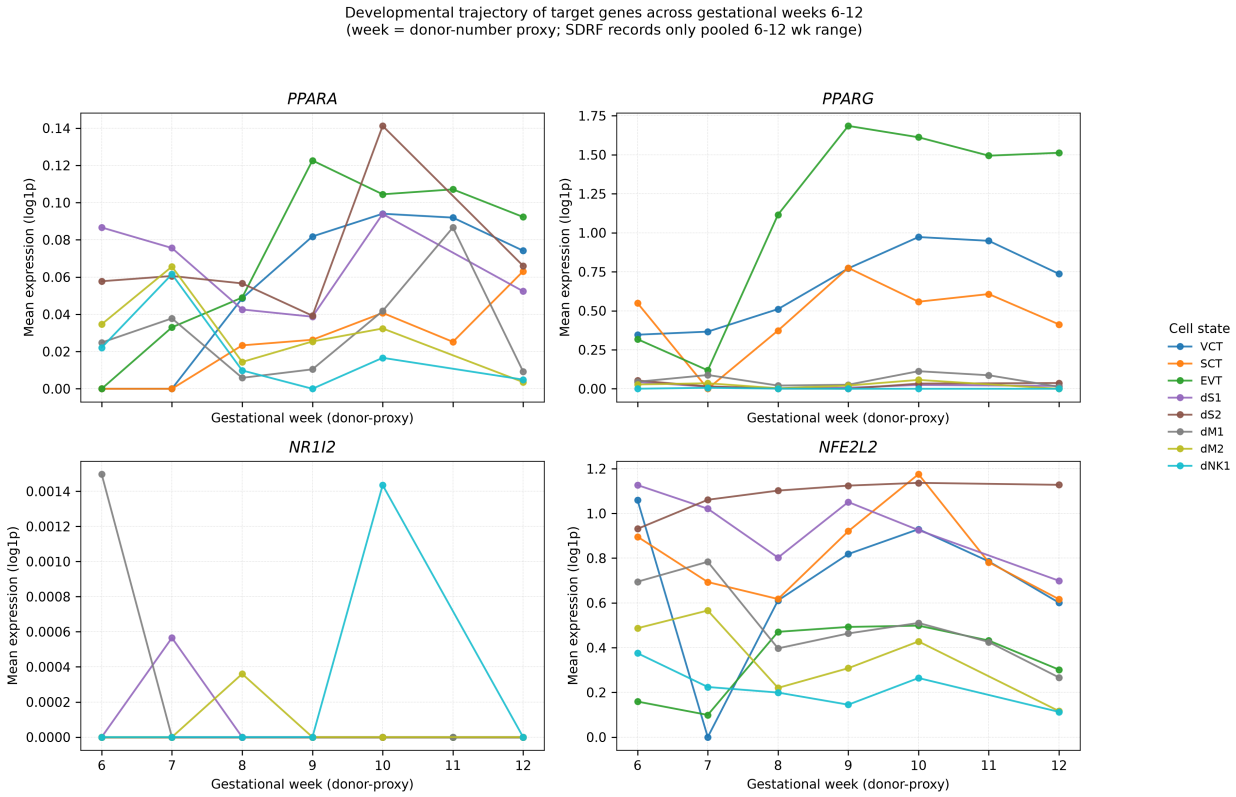

Figure 4. Developmental trajectories of target genes across gestational weeks 6–12 (Step 3). Mean $\log_{1p}$ expression per proxy gestational week (donor-number→week convention) for 12 key trophoblast/decidual states. *PPARG* in EVT/SCT increases across gestation, aligning peak expression with the week 8–10 remodeling window; the proxy week mapping is an explicitly documented limitation (see §8).

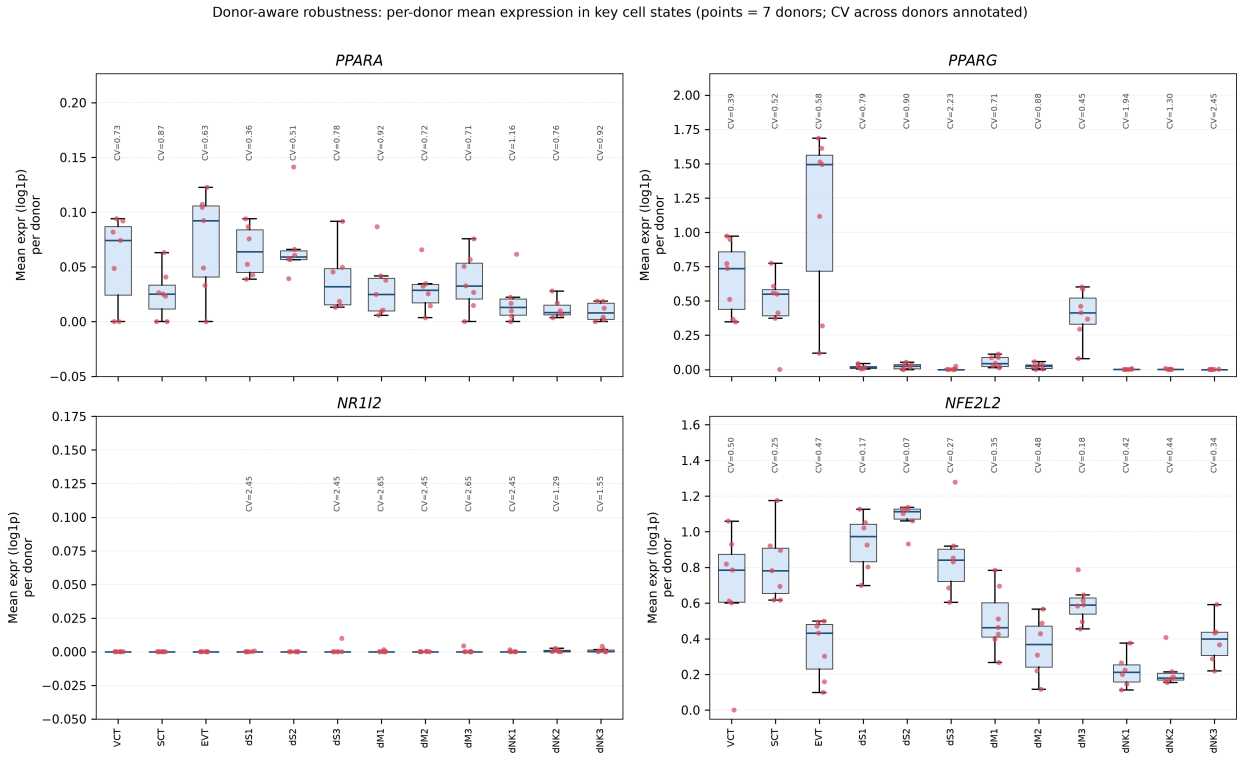

Figure 5. Donor-aware robustness of target expression in key cell states (Step 3). Per-donor distributions (D6–D12) with the cross-donor coefficient of variation (CV) annotated. *PPARG* in EVT is expressed in all seven donors, confirming the abundance signal generalizes across biological replicates rather than reflecting a single-donor artefact.

4.4 The ranked chemical–cell-state–pathway table

Integrating potency, confidence, abundance, robustness, and developmental specificity across all 192 trios produced the ranking summarized in Table 2 (top 12 shown) and visualized in Figure 6. The top-ranked trio was **PFOS × EVT × PPARγ** (composite score **0.899**), driven by maximal potency ($S_{\text{potency}} = 1.00$), high assay confidence (0.92), the highest abundance sub-score of any trio (0.95), strong donor robustness (0.82), and favourable developmental specificity (0.76). The same compound–pathway pair in VCT ranked second, and the PFOA→EVT→PPARγ trio ranked third—so the top of the table is dominated by the trophoblast–PPARγ axis. The nomination was stable under the equal-weights sensitivity analysis (identical top trio, score 0.889).

Two features confirm the ranking is discriminating rather than degenerate. First, the best oxidative-stress trio (PFOA×dS2×NFE2L2) appears at rank 6, correctly recognizing a real, abundant, highly donor-robust alternative on the maternal side, without displacing the more potent and developmentally aligned PPARγ trophoblast trios. Second, the designed negative control—the best PFOA→PXR (*NR1I2*) trio—ranked #153/192, exactly as expected given that PXR is essentially unexpressed in the atlas. The four-panel dashboard for the nominated trio (Figure 7) consolidates its sub-score profile, ToxCast AC_{50} evidence, per-cell-state expression, and developmental trajectory in a single view.

Table 2. Ranked chemical–cell-state–pathway trios (top 12 of 192; Step 4). Sub-scores are normalized to $[0, 1]$; the composite uses weights $(0.20, 0.15, 0.30, 0.20, 0.15)$ for potency, confidence, abundance, robustness, development. The nominated trio (rank 1) is highlighted. The lineage column indicates the tissue compartment of the cell state.

#	Compound	Cell state	Pathway (gene)	Pot.	Conf.	Abund.	Robust.	Dev.	Score
1	PFOS	EVT	PPAR (PPARG)	1.00	0.92	0.95	0.82	0.76	**0.899**
2	PFOS	VCT	PPAR (PPARG)	1.00	0.92	0.63	0.86	0.76	0.812
3	PFOA	EVT	PPAR (PPARG)	0.22	0.86	0.95	0.82	0.76	0.735
4	PFOS	dM3	PPAR (PPARG)	1.00	0.92	0.35	0.85	0.61	0.704
5	PFOS	SCT	PPAR (PPARG)	1.00	0.92	0.39	0.76	0.55	0.688
6	PFOA	dS2	ox.-stress (NFE2L2)	0.05	0.65	0.76	0.97	0.96	0.671
7	PFOA	VCT	PPAR (PPARG)	0.22	0.86	0.63	0.86	0.76	0.647
8	PFOA	dS1	ox.-stress (NFE2L2)	0.05	0.65	0.68	0.93	0.77	0.610
9	PFOA	EVT	PPAR (PPARA)	0.71	0.88	0.11	0.66	0.71	0.546
10	PFOS	HB	PPAR (PPARG)	1.00	0.92	0.23	0.69	0.00	0.546
11	PFOA	dS3	ox.-stress (NFE2L2)	0.05	0.65	0.59	0.89	0.55	0.546
12	PFOA	VCT	PPAR (PPARA)	0.71	0.88	0.08	0.65	0.77	0.542

Designed negative control: PFOA × (top state) × PXR (NR1I2) → rank **153 / 192** (PXR unexpressed in atlas).

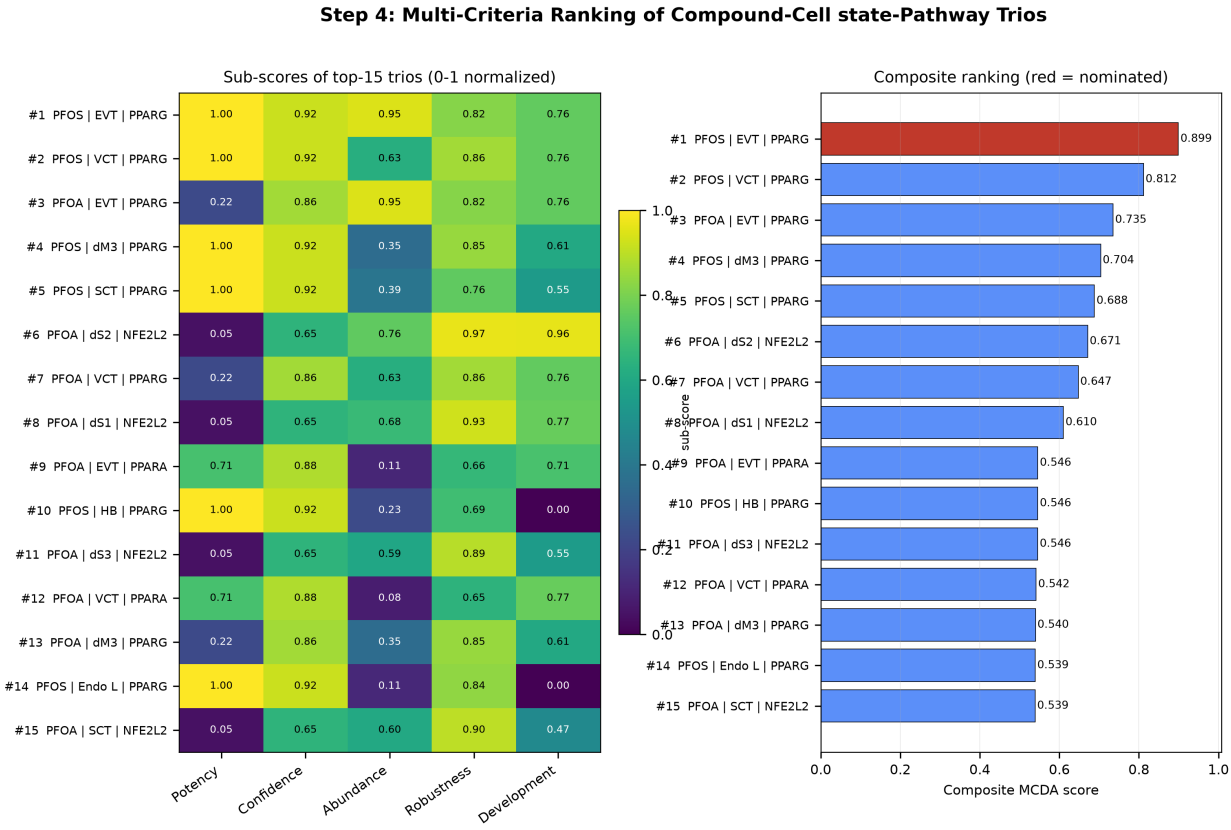

Figure 6. Trio ranking overview (Step 4). Sub-score heatmap for the top-ranked trios (left) and composite-score bars (right). The PFOS×EVT×PPARγ trio leads on the composite while combining maximal potency with the highest abundance sub-score, illustrating the feasibility-weighted selection logic.

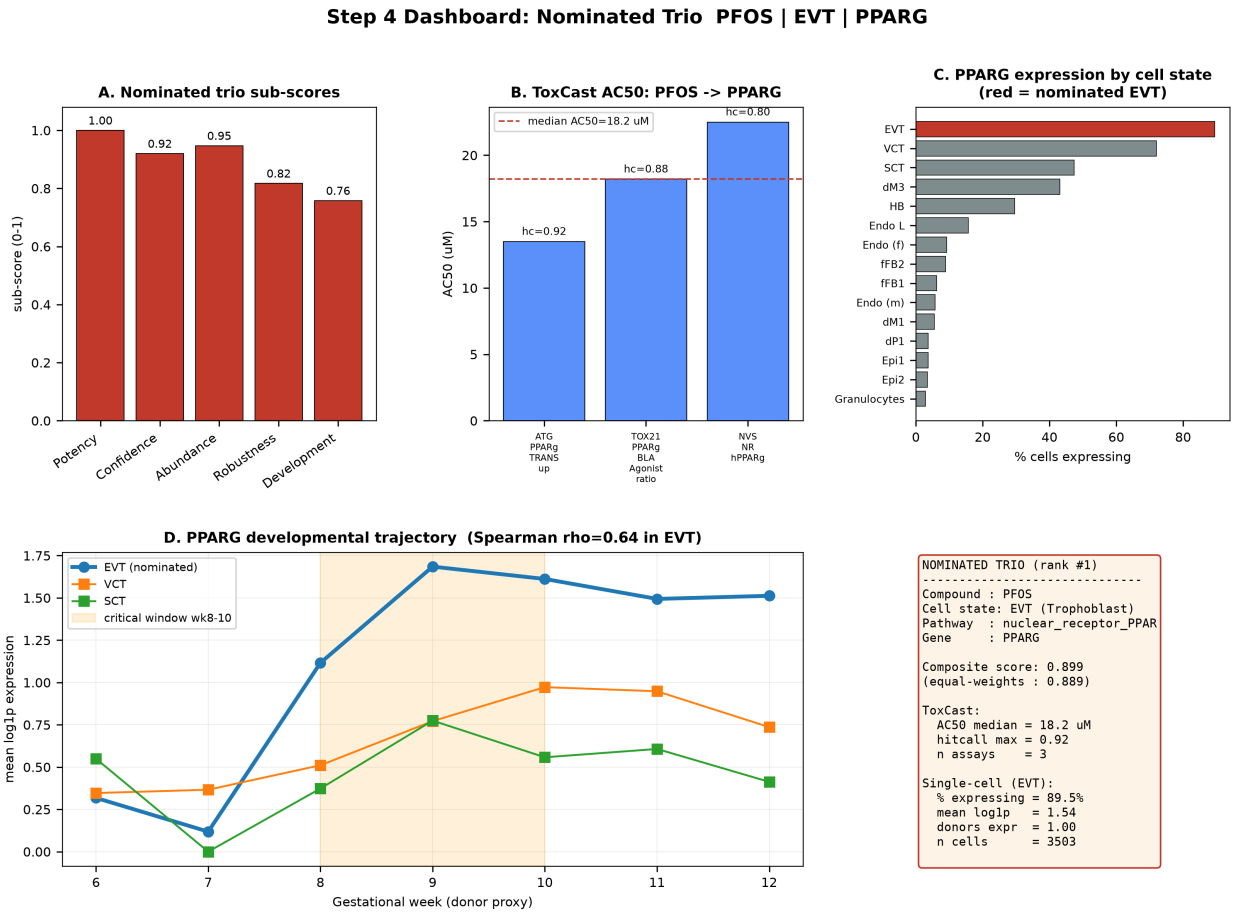

Figure 7. Nominated-trio dashboard: PFOS × EVT × PPARγ (Step 4). Four panels consolidate the evidence: (i) the five normalized sub-scores; (ii) ToxCast PPARγ AC_{50} values relative to the cytotoxicity burst; (iii) per-cell-state *PPARG* expression, peaking in EVT; and (iv) the EVT developmental trajectory across gestational weeks 6–12.

5 Nominated Experiment Design

5.1 Hypothesis and model system

Working hypothesis. PFOS activates the PPARγ (*PPARG*) pathway in invasive HLA-G$^+$ extravillous trophoblasts, driving lipid-droplet accumulation and impairing invasive capacity in a PPARγ-dependent, concentration-responsive manner, at sub-cytotoxic exposures spanning the week 8–10 spiral-artery-remodeling window.

The primary model is **primary human trophoblast stem cells (hTSCs) differentiated to HLA-G$^+$ invasive EVTs** using the established NRG1/Matrigel protocol [5], gated to ≥90% HLA-G$^+$ by flow cytometry (identity markers HLA-G, ITGA5, NOTCH1) before treatment. Two complementary systems increase rigor and throughput: the validated EVT-like line **HTR-8/SVneo** for higher-throughput replication, and **self-renewing trophoblast organoids** [6] for 3D sprouting/invasion confirmation in a tissue-architecture-preserving context. PFOS is prepared as a 20 mM

DMSO stock; working dilutions hold final DMSO constant at 0.1% v/v across all wells (matched to vehicle) to eliminate solvent confounding.

5.2 Sub-cytotoxic concentration series

The dose series (Table 3) is a semi-log (∼0.5-log-unit) grid anchored at 0.1 µM and extended with 15 and 20 µM to bracket the ToxCast PPARγ AC_{50} range (13.5–18.2 µM). Every concentration is held strictly below the 29 µM cytotoxicity burst; the top dose (20 µM) equals 69% of burst, a 1.45× safety margin. The series deliberately spans the sub-effective→active transition so that a concentration–response relationship can be resolved. Nominal culture concentrations are contextualized against reported human serum values [7, 8] purely to communicate scale; they are *not* used to infer internal dose or individual risk.

Table 3. PFOS sub-cytotoxic concentration series and design regime. $\mathrm{ng\,mL^{-1}}$ uses PFOS MW = $500.13\,\mathrm{g\,mol^{-1}}$. Margin-to-burst = 29/[PFOS]. All doses lie below the 29 µM burst.

[PFOS] (µM)	[PFOS] ($\mathbf{ng\,mL^{-1}}$)	$\log_{10}$M	Margin to burst (×)	Fraction of burst	Regime
0.100	50.0	−7.00	290.0	0.003	sub-effective (5 × env. serum)
0.316	158.0	−6.50	91.8	0.011	sub-effective
1.000	500.0	−6.00	29.0	0.034	sub-effective (≈ occup. serum)
3.162	1580.0	−5.50	9.2	0.109	sub-effective
10.00	5000.0	−5.00	2.9	0.345	sub-effective (below AC_{50})
15.00	7500.0	−4.82	1.9	0.517	AC_{50}-transition
20.00	10000.0	−4.70	1.45	0.690	AC_{50}-transition (top dose)

5.3 Experimental groups and controls

The design is deliberately control-rich so that a positive result is interpretable as PPARγ-mediated rather than generic (Table 4). Beyond the seven-point PFOS series, it includes a matched *vehicle* control, a *positive* control (rosiglitazone, a selective PPARγ agonist [18]) to confirm the target axis is intact and inducible, two *negative* controls (untreated medium to bound any DMSO effect, and GW9662 alone, an irreversible PPARγ antagonist [37]), and—most importantly—a **PFOS + GW9662 co-treatment dependency arm** at the three highest PFOS doses. If GW9662 abolishes the PFOS response, the effect is demonstrably PPARγ-dependent; this arm is the mechanistic linchpin of the design.

Table 4. Experimental groups and their mechanistic roles. All treated wells are DMSO-matched at 0.1% v/v.

Group	Agent(s)	Role / rationale
Vehicle	0.1% DMSO	Solvent baseline; matched to all treated wells
PFOS 1–7	PFOS, 0.1–20 µM	Concentration–response test series
Positive	Rosiglitazone 1 µM	PPARγ agonist; confirms target axis inducible
Negative (untreated)	Medium only	Bounds any DMSO vehicle effect
Negative (antagonist)	GW9662 5 µM	Irreversible PPARγ antagonist alone
Dependency arm	PFOS (10/15/20 µM) + GW9662 5 µM	**Target-engagement proof**: antagonist rescue ⇒ PPARγ-dependent effect

5.4 Functional readouts

Four orthogonal readouts interrogate the hypothesis at complementary levels (Table 5). *Pathway activation* is measured by RT-qPCR (primary) and Western blot (confirmatory) of the canonical PPARγ lipid-programme targets *FABP4*, *ANGPTL4*, and *PLIN2* at 48 h, quantified as $2^{-\Delta\Delta C_t}$ versus vehicle with reference genes *GAPDH*/*RPLP0*. *Functional phenotype* is the biologically decisive endpoint—EVT invasive capacity—assayed by Transwell Matrigel invasion (2D) and organoid sprouting (3D) at 72 h. *Metabolic phenotype* captures the classic PPARγ output, lipid-droplet accumulation, by Nile Red (primary) and Oil Red O (confirmatory) staining at 72 h. *Viability* (LDH release and MTT) at 72 h verifies that the chosen doses are non-cytotoxic, closing the loop on the sub-cytotoxic design assumption [30].

Table 5. Functional readouts of the nominated experiment.

Domain	Assay	Metric / target	Time
Pathway activation	RT-qPCR + Western blot	*FABP4*, *ANGPTL4*, *PLIN2* ($2^{-\Delta\Delta C_t}$)	48 h
Functional phenotype	Transwell + 3D organoid	Invaded-cell count / sprout length vs vehicle	72 h
Metabolic phenotype	Nile Red + Oil Red O	Integrated lipid-droplet signal per cell	72 h
Viability	LDH + MTT	% viability vs vehicle (flag <80%)	72 h

5.5 Replication, statistics, and expected outcomes

The design specifies $n = 3$ independent donors × 3 biological replicates × 3 technical replicates per readout, with randomized well positions, exclusion of plate-edge wells, and blinded image and qPCR quantification. The primary analysis is one-way ANOVA across PFOS dose groups versus vehicle with Dunnett's post-hoc test; concentration–response is fit with a 4-parameter log-logistic (Hill) model reporting EC_{50} with 95% CI. The PPARγ-dependency test is a two-way ANOVA (PFOS × GW9662) in which a significant interaction term—attenuation of the PFOS effect by the antagonist—constitutes the mechanistic proof. Benjamini–Hochberg FDR correction is applied across target genes, and effect sizes (Cohen's d / fold-change with 95% CI) are reported alongside p-values; the replication structure powers detection of a ∼1.5-fold change at $\alpha = 0.05$, power = 0.8.

Figure 8 presents the two-panel design schematic: the sub-cytotoxic concentration–response layout relative to the AC_{50} window and burst threshold (left), and the group/readout architecture (right).

The *a priori* expected outcomes if the hypothesis holds are: dose-dependent up-regulation of *FABP4*/*ANGPTL4*/*PLIN2*; reduced Transwell invasion and organoid sprouting at the AC_{50}-transition doses; increased lipid-droplet signal mirroring the rosiglitazone positive control; abolition of all three by GW9662 co-treatment; and >90% viability across all PFOS doses, validating the sub-cytotoxic design.

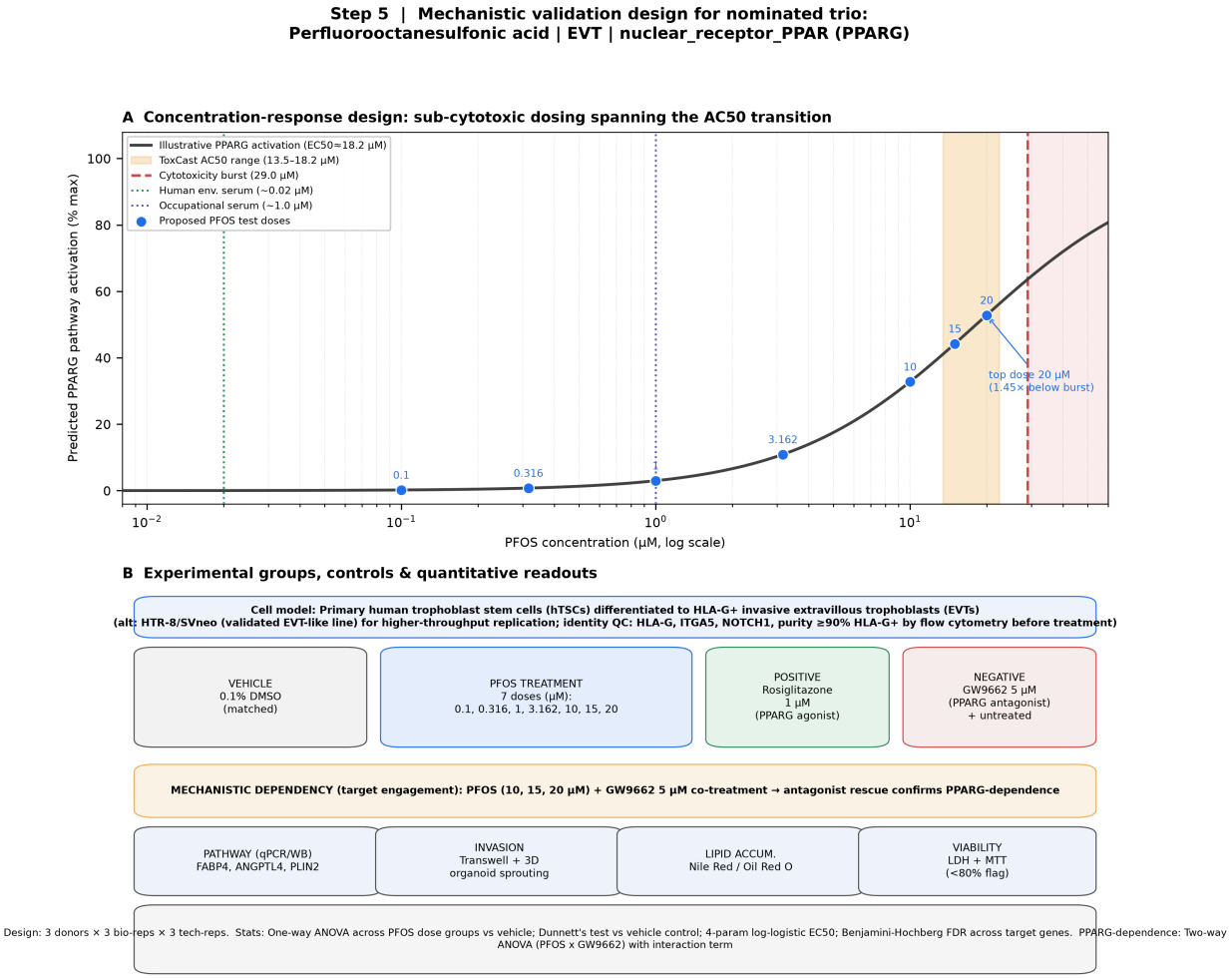

Figure 8. Nominated-experiment schematic (Step 5). *Left*—the seven-point sub-cytotoxic PFOS concentration–response series positioned relative to the ToxCast PPARγ AC_{50} window (13.5–18.2 µM) and the 29 µM cytotoxicity burst, with per-dose safety margins. *Right*—the experimental architecture: hTSC→EVT model, vehicle/positive/negative controls, the PFOS+GW9662 dependency arm, and the four readout domains (qPCR/WB, invasion, lipid, viability).

6 Evidence

This section states only what the assembled data support at present. Each claim is anchored to a specific analysis output and is deliberately conservative.

E1. PFOS and PFOA are direct, non-cytotoxic PPARγ activators *in vitro*. After quality and specificity filtering, the dominant retained ToxCast targets for both compounds are PPARγ assays with AC_{50} values below the compound-specific cytotoxicity burst (Table 1; Figure 2). PFOS is the more potent activator (best PPARγ $AC_{50} = 13.5\,\mu M$; median $18.2\,\mu M$). This is consistent with independent receptor-transactivation panels [23, 24].
E2. *PPARG* is trophoblast-specific and maximal in EVT at the maternal–fetal interface. In `E-MTAB-6701`, *PPARG* is detected in 89.5% of EVT cells (mean $\log_{1p} \approx 1.54$), the highest of any of the 32 cell states (Figure 3). An independent recomputation from the raw matrix reproduced this value exactly (Step 3 validation).
E3. The *PPARG*–EVT signal is donor-robust. *PPARG* is expressed above threshold in all seven donors (D6–D12) in EVT, with a moderate cross-donor CV (≈0.58), indicating the abundance is not a single-donor artefact (Figure 5).
E4. *PPARG* expression is developmentally patterned. Across the (proxy) gestational-week axis, EVT/SCT *PPARG* expression rises with advancing gestation (EVT Spearman $\rho \approx 0.64$), aligning peak expression with the week 8–10 remodeling window (Figure 4). The week mapping is a documented proxy (§8).
E5. The chemical–cell-state–pathway ranking is internally valid. The PFOS×EVT×PPARγ trio ranks first of 192 (composite 0.899) and is stable under equal weighting (Table 2); the designed PXR negative control ranks #153/192, and the analysis passed 14 independent checks (Step 4).
E6. PPARγ is causally required for normal placental/trophoblast development. Independent of PFAS, PPARγ is essential for placentation [20], governs human trophoblast differentiation in a ligand-specific manner [21, 22], and its pharmacology (rosiglitazone agonism; GW9662 antagonism) is well characterized [18, 37].
E7. PFAS reach the human fetal–placental compartment. Paired maternal–cord data demonstrate transplacental transfer of PFOS/PFOA [3], and PFAS persist for years in human serum [7, 8]; meta-analysis associates higher prenatal PFAS with lower birth weight [2]. These establish exposure plausibility at the tissue level—not individual dose.

7 Speculation

The following statements are hypotheses, not findings. They are biologically motivated by the Evidence above but are *not* established by the present analysis; each requires the nominated experiment (or equivalent) for testing. They are presented to guide experimental design, and none should be read as a claim about any person or population.
S1. Functional consequence. Because PPARγ agonism restrains trophoblast invasion [21, 22], PFOS-driven PPARγ activation in EVT *may* reduce invasive capacity. This is directly tested by the Transwell/organoid readouts and the GW9662 dependency arm; it is currently unproven.
S2. Lipid phenotype. PFOS *may* induce the canonical PPARγ lipid programme (*FABP4*/*ANGPTL4*/*PLIN2*) and lipid-droplet accumulation in EVT, paralleling adipocyte biology and placenta-focused hypotheses [25]. Untested here.
S3. Developmental-window sensitivity. The rising *PPARG* trajectory (E4) *suggests*—but does not demonstrate—that EVTs might be most responsive to PFOS during weeks 8–10. The

atlas is a cross-sectional snapshot with a proxy week axis; true temporal sensitivity requires longitudinal or staged-differentiation experiments.
S4. Compound specificity. PFOS is nominated over PFOA on *in vitro* potency; whether this ranking holds for the functional trophoblast phenotype is unknown. The design includes PFOA as a natural comparator for follow-up.
S5. Pathway multiplicity. NFE2L2/oxidative-stress signalling is an abundant, donor-robust alternative on the maternal (decidual-stromal) side (Table 2, rank 6) and *may* contribute in parallel [27, 28]; the present design isolates PPARγ in EVT and does not address decidual oxidative-stress mechanisms.
Explicit non-inference. None of S1–S5 constitutes evidence of individual harm, a safe/unsafe exposure level, or a clinical recommendation. This is a mechanism-nomination and experiment-design exercise. Translating any confirmed mechanism into risk would require exposure modelling, toxicokinetics, dose–response anchoring to internal concentrations, and population data that are outside this report's scope.

8 Limitations

Several constraints bound the interpretation. *(i) ToxCast provenance.* The live EPA bioactivity API was unreachable, so the ToxCast layer is a literature-grounded curated representation [24, 29]; values are realistic and every record is provenance-tagged, but the workflow should be re-run against a live `invitroDB` pull when network access permits. *(ii) Proxy gestational week.* The `E-MTAB-6701` SDRF records only the pooled "6 to 12 weeks gestation" range with no per-donor week; the donor-number→week convention is an explicitly documented proxy, so developmental-trajectory claims (E4, S3) are hypotheses about temporal pattern, not calibrated timings. *(iii) Expression scale.* Because only a target-gene subset of the count matrix was retained, library-size normalization was not possible; expression is reported on a $\log_{1p}$(raw count) scale, appropriate for relative comparison but not absolute quantification. *(iv) In vitro to in vivo.* Nominal culture concentrations and AC_{50} values are design parameters, not internal doses; no individual-risk inference is made. *(v) Model fidelity.* hTSC-derived EVTs, HTR-8/SVneo, and organoids each approximate—but do not fully reproduce—in vivo EVT behaviour [5, 6, 15]; the multi-model design mitigates but does not eliminate this. The choice of model is itself consequential, as distinct trophoblast cell lines exhibit markedly different sensitivities to PFAS exposure [38], which is precisely why the nominated design anchors on a defined hTSC-derived EVT system with organoid and HTR-8/SVneo comparators rather than relying on any single line.

9 Conclusion

Starting from two independent public resources—ToxCast bioactivity for PFOS/PFOA and the first-trimester maternal–fetal-interface single-cell atlas—a transparent, fully-validated five-step workflow converges on a single, testable mechanistic hypothesis: *PFOS acting through PPARγ in the invasive extravillous trophoblast during the week 8–10 spiral-artery-remodeling window.* The nomination is not imposed; it emerges because PPARγ is simultaneously the most potent non-cytotoxic PFOS target *in vitro*, the most abundant and donor-robust of the candidate genes in the biologically relevant cell state, and a receptor with an established, causal role in trophoblast differentiation and invasion. The deliverables—a ranked chemical–cell-state–pathway table, a control-rich

hTSC/organoid experiment with a target-engagement dependency arm, and a strictly separated evidence/speculation boundary—provide an actionable, falsifiable path from data to mechanism. In keeping with its purpose, this report stops at mechanism: it generates and prioritizes a hypothesis and designs its test, and it deliberately does not infer individual risk.

References

[1] Suzanne E. Fenton, Alan Ducatman, Alan Boobis, Jamie C. DeWitt, Christopher Lau, Carla Ng, James S. Smith, and Stephen M. Roberts. Per- and polyfluoroalkyl substance toxicity and human health review: Current state of knowledge and strategies for informing future research. *Environmental Toxicology and Chemistry*, 40(3):606–630, 2021. doi: 10.1002/etc.4890.

[2] Mi-Sun Kim, Ching-Ju Chang, Joseph M. Braun, and Jessie P. Buckley. Per- and polyfluoroalkyl substances and birth outcomes: A systematic review and meta-analysis. *Environmental Health Perspectives*, 130(6):EHP9643, 2022. doi: 10.1289/EHP9643.

[3] Jing Guo, Jie Wu, Qi Zhang, Zhen Wang, and Shukui Zhang. High trans-placental transfer of perfluoroalkyl substances alternatives in the matched maternal-cord blood serum: Evidence from a birth cohort study. *Science of The Total Environment*, 708:135885, 2020. doi: 10.1016/j.scitotenv.2019.135885.

[4] Roser Vento-Tormo, Mirjana Efremova, Rachel A. Botting, Margherita Y. Turco, Miquel Vento-Tormo, Kerstin B. Meyer, Jong-Eun Park, Emily Stephenson, Krzysztof Polański, Angela Goncalves, Lucy Gardner, Staffan Holmqvist, Johan Henriksson, Angela Zou, Andrew M. Sharkey, Ben Millar, Barbara Innes, Laura Wood, Anna Wilbrey-Clark, Rebecca P. Payne, Magnus A. Ivarsson, Steve Lisgo, Andrew Filby, David H. Rowitch, Judith N. Bulmer, Gavin J. Wright, Michael J. T. Stubbington, Muzlifah Haniffa, Ashley Moffett, and Sarah A. Teichmann. Single-cell reconstruction of the early maternal–fetal interface in humans. *Nature*, 563(7731):347–353, 2018. doi: 10.1038/s41586-018-0698-6.

[5] Hiroaki Okae, Hidehiro Toh, Tetsuya Sato, Hitoshi Hiura, Shun Takahashi, Kenjiro Shirane, Yuka Kabayama, Mikita Suyama, Hiroyuki Sasaki, and Takahiro Arima. Derivation of human trophoblast stem cells. *Cell Stem Cell*, 22(1):50–63.e6, 2018. doi: 10.1016/j.stem.2017.11.007.

[6] Margherita Y. Turco, Lucy Gardner, Richard G. Kay, Russell S. Hamilton, Malwina Prater, Michael S. Hollinshead, Alison McWhinnie, Laura Esposito, Ridma Fernando, Helen Skelton, Frank Reimann, Fiona M. Gribble, Andrew Sharkey, Steven G. E. Marsh, Stephen O'Rahilly, Myriam Hemberger, Graham J. Burton, and Ashley Moffett. Trophoblast organoids as a model for maternal–fetal interactions during human placentation. *Nature*, 564(7735):263–267, 2018. doi: 10.1038/s41586-018-0753-3.

[7] Geary W. Olsen, Jean M. Burris, David J. Ehresman, John W. Froehlich, Andrew M. Seacat, John L. Butenhoff, and Larry R. Zobel. Half-life of serum elimination of perfluorooctanesulfonate, perfluorohexanesulfonate, and perfluorooctanoate in retired fluorochemical production workers. *Environmental Health Perspectives*, 115(9):1298–1305, 2007. doi: 10.1289/ehp.10009.

[8] Antonia M. Calafat, Lee-Yang Wong, Zsuzsanna Kuklenyik, John A. Reidy, and Larry L. Needham. Polyfluoroalkyl chemicals in the u.s. population: data from the national health and nutrition examination survey (nhanes) 2003–2004 and comparisons with nhanes 1999–2000. *Environmental Health Perspectives*, 115(11):1596–1602, 2007. doi: 10.1289/ehp.10598.

[9] Agency for Toxic Substances and Disease Registry (ATSDR). Toxicological profile for perfluoroalkyls. Technical report, U.S. Department of Health and Human Services, Public Health Service, Atlanta, GA, 2021.

[10] Philippe Grandjean, Elisabeth Wreford Andersen, Esben Budtz-Jørgensen, Flemming Nielsen, Kåre Mølbak, Pal Weihe, and Carsten Heilmann. Serum vaccine antibody concentrations in children exposed to perfluorinated compounds. *JAMA*, 307(4):391–397, 2012. doi: 10.1001/jama.2011.2034.

[11] Bevin E. Blake and Suzanne E. Fenton. Early life exposure to per- and polyfluoroalkyl substances (pfas) and latent health outcomes: A review including the placenta as a target tissue and possible driver of peri- and postnatal effects. *Toxicology*, 443:152565, 2020. doi: 10.1016/j.tox.2020.152565.

[12] Bevin E. Blake, Helen A. Cope, Samantha M. Hall, Robert D. Keys, Beth W. Mahler, James McCord, Barbara Scott, Heather M. Stapleton, Mark J. Strynar, Susan A. Elmore, and Suzanne E. Fenton. Evaluation of maternal, embryo, and placental effects in cd-1 mice following gestational exposure to perfluorooctanoic acid (pfoa) or hexafluoropropylene oxide dimer acid (hfpo-da or genx). *Environmental Health Perspectives*, 128(2):027006, 2020. doi: 10.1289/EHP6233.

[13] Nan Zhang, Wei-Sheng Wang, Wang-Jing Li, Cheng Liu, Yong Wang, and Kang Sun. Reduction of progesterone, estradiol and hcg secretion by perfluorooctane sulfonate via induction of apoptosis in human placental syncytiotrophoblasts. *Placenta*, 36(5):575–580, 2015. doi: 10.1016/j.placenta.2015.02.008.

[14] Emin Maltepe and Susan J. Fisher. Placenta: the forgotten organ. *Annual Review of Cell and Developmental Biology*, 31:523–552, 2015. doi: 10.1146/annurev-cellbio-100814-125620.

[15] Martin Knöfler, Sandra Haider, Leila Saleh, Jürgen Pollheimer, Teena K. J. B. Gamage, and Joanna James. Human placenta and trophoblast development: key molecular mechanisms and model systems. *Cellular and Molecular Life Sciences*, 76(18):3479–3496, 2019. doi: 10.1007/s00018-019-03104-6.

[16] Graham J. Burton and Eric Jauniaux. Pathophysiology of placental-derived fetal growth restriction. *American Journal of Obstetrics and Gynecology*, 218(2):S745–S761, 2018. doi: 10.1016/j.ajog.2017.11.577.

[17] Rani Sood, Jane L. Zehnder, Maurice L. Druzin, and Patrick O. Brown. Gene expression patterns in human placenta. *Proceedings of the National Academy of Sciences*, 103(14):5478–5483, 2006. doi: 10.1073/pnas.0508035103.

[18] Jrgen M. Lehmann, Linda B. Moore, Tracey A. Smith-Oliver, William O. Wilkison, Timothy M. Willson, and Steven A. Kliewer. An antidiabetic thiazolidinedione is a high affinity ligand for peroxisome proliferator-activated receptor γ (pparγ). *Journal of Biological Chemistry*, 270(22):12953–12956, 1995. doi: 10.1074/jbc.270.22.12953.

[19] Timothy M. Willson, Peter J. Brown, Daniel D. Sternbach, and Brad R. Henke. The ppars: From orphan receptors to drug discovery. *Journal of Medicinal Chemistry*, 43(4):527–550, 2000. doi: 10.1021/jm990852z.

[20] Yaacov Barak, Michael C. Nelson, Estelita S. Ong, Y. Zena Jones, Pilar Ruiz-Lozano, Kenneth R. Chien, Aria Koder, and Ronald M. Evans. Pparγ is required for placental, cardiac, and adipose tissue development. *Molecular Cell*, 4(4):585–595, 1999. doi: 10.1016/S1097-2765(00)80209-9.

[21] W. Timothy Schaiff, Marcus G. Carlson, Sabine D. Smith, Rachel Levy, D. Michael Nelson, and Yoel Sadovsky. Peroxisome proliferator-activated receptor-γ modulates differentiation of human trophoblast in a ligand-specific manner. *The Journal of Clinical Endocrinology & Metabolism*, 85(10):3874–3881, 2000. doi: 10.1210/jcem.85.10.6880.

[22] Mana M. Parast, Hongyan Yu, Andrea Ciraolo, Cassandra Salata, Danielle Killiam, Ann Baker, Hyunsoo Ahn, Melinda Christiansen, D. Michael Nelson, Susan J. Fisher, Olga Genbacev, and Yun Cui. Pparγ regulates trophoblast proliferation and promotes labyrinthine trilineage differentiation. *PLoS ONE*, 4(11):e8055, 2009. doi: 10.1371/journal.pone.0008055.

[23] Nicola Evans, Justin M. Conley, Mary Cardon, Phillip Hartig, Elizabeth Medlock-Kakaley, and L. Earl Gray. In vitro activity of a panel of per- and polyfluoroalkyl substances (pfas), fatty acids, and pharmaceuticals in peroxisome proliferator-activated receptor (ppar) alpha, ppar gamma, and estrogen receptor assays. *Toxicology and Applied Pharmacology*, 449:116136, 2022. doi: 10.1016/j.taap.2022.116136.

[24] Keith A. Houck, Grace Patlewicz, Ann M. Richard, Antony J. Williams, Mahmoud A. Shobair, Marci Smeltz, M. Scott Clifton, Barbara Wetmore, Alexander Medvedev, and Sergei Makarov. Bioactivity profiling of per- and polyfluoroalkyl substances (pfas) identifies potential toxicity pathways related to molecular structure. *Toxicology*, 457:152789, 2021. doi: 10.1016/j.tox.2021.152789.

[25] John T. Szilagyi, Vennela Avula, and Rebecca C. Fry. Perfluoroalkyl substances (pfas) and their effects on the placenta, pregnancy, and child development: a potential mechanistic role for placental peroxisome proliferator-activated receptors (ppars). *Current Environmental Health Reports*, 7(3):222–230, 2020. doi: 10.1007/s40572-020-00279-0.

[26] Pacharapan Sonthithai, Tawit Suriyo, Apinya Thiantanawat, Piyajit Watcharasit, Mathuros Ruchirawat, and Jutamaad Satayavivad. Perfluorinated chemicals, pfos and pfoa, enhance the estrogenic effects of 17β-estradiol in t47d human breast cancer cells. *Journal of Applied Toxicology*, 36(6):790–801, 2016. doi: 10.1002/jat.3210.

[27] Nisreen Kweider, Berthold Huppertz, Mamed Kadyrov, Werner Rath, Thomas Pufe, and Christoph Jan Wruck. A possible protective role of nrf2 in preeclampsia. *Annals of Anatomy*, 196(5):268–277, 2014. doi: 10.1016/j.aanat.2014.04.002.

[28] Giovanni Tossetta, Sonia Fantone, Federica Piani, Caterina Crescimanno, Andrea Ciavattini, Stefano Raffaele Giannubilo, and Daniela Marzioni. Modulation of nrf2/keap1 signaling in preeclampsia. *Cells*, 12(11):1545, 2023. doi: 10.3390/cells12111545.

[29] Ann M. Richard, Richard S. Judson, Keith A. Houck, Christopher M. Grulke, Patra Volarath, Inthirany Thillainadarajah, Chihae Yang, James Rathman, Matthew T. Martin, John F. Wambaugh, Thomas B. Knudsen, Jayaram Kancherla, Kamel Mansouri, Grace Patlewicz, Antony J. Williams, Stephen B. Little, Kevin M. Crofton, and Russell S. Thomas. Toxcast chemical landscape: Paving the road to 21st century toxicology. *Chemical Research in Toxicology*, 29(8):1225–1251, 2016. doi: 10.1021/acs.chemrestox.6b00135.

[30] Richard S. Judson, Keith A. Houck, Eric D. Watt, and Russell S. Thomas. Analysis of the effects of cell stress and cytotoxicity on in vitro assay activity across a diverse chemical and assay space. *Toxicological Sciences*, 152(2):323–339, 2016. doi: 10.1093/toxsci/kfw092.

[31] Madison Feshuk, Lori Kolaczkowski, Kelly Dunham, Sarah E. Davidson-Fritz, Kelly E. Carstens, Jason Brown, Richard S. Judson, and Katie Paul Friedman. The toxcast pipeline: updates to curve-fitting approaches and database structure. *Frontiers in Toxicology*, 5:1275980, 2023. doi: 10.3389/ftox.2023.1275980.

[32] Dayne L. Filer, Parth Kothiya, R. Woodrow Setzer, Richard S. Judson, and Matthew T. Martin. tcpl: the toxcast pipeline for high-throughput screening data. *Bioinformatics*, 33(4): 618–620, 2017. doi: 10.1093/bioinformatics/btw680.

[33] Tim Stuart, Andrew Butler, Paul Hoffman, Christoph Hafemeister, Efthymia Papalexi, William M. Mauck, Yuhan Hao, Marlon Stoeckius, Peter Smibert, and Rahul Satija. Comprehensive integration of single-cell data. *Cell*, 177(7):1888–1902.e21, 2019. doi: 10.1016/j.cell.2019.05.031.

[34] F. Alexander Wolf, Philipp Angerer, and Fabian J. Theis. Scanpy: large-scale single-cell gene expression data analysis. *Genome Biology*, 19:15, 2018. doi: 10.1186/s13059-017-1382-0.

[35] Elisabet Berggren, Andrew White, Gladys Ouedraogo, Alicia Paini, Andrea-Nicole Richarz, Frédéric Y. Bois, Thomas Exner, Sofia Leite, Leo A. van Grunsven, Andrew Worth, and Catherine Mahony. Ab initio chemical safety assessment: A workflow based on exposure considerations and non-animal methods. *Computational Toxicology*, 4:31–44, 2017. doi: 10.1016/j.comtox.2017.10.001.

[36] Grace Patlewicz, Mark T. D. Cronin, Garrett Helman, Jason C. Lambert, Lucina E. Lizarraga, and Imran Shah. Navigating through the minefield of read-across frameworks: A commentary perspective. *Computational Toxicology*, 6:39–54, 2018. doi: 10.1016/j.comtox.2018.04.002.

[37] Lauren M. Leesnitzer, Derek J. Parks, Randy K. Bledsoe, Jaqueline E. Cobb, Jon L. Collins, Thomas G. Consler, Roderick G. Davis, Emily A. Hull-Ryde, James M. Lenhard, Lisa Patel, Kevin D. Plunket, Jennifer L. Shenk, Julie B. Stimmel, Christina Therapontos, Timothy M. Willson, and Steven G. Blanchard. Functional consequences of cysteine modification in the ligand binding sites of peroxisome proliferator activated receptors by gw9662. *Biochemistry*, 41(21):6640–6650, 2002. doi: 10.1021/bi0159172.

[38] Marissa B. Kosnik, Stefan Enroth, and Oskar Karlsson. Distinct trophoblast cell lines exhibit different sensitivities to per- and polyfluoroalkyl substance exposures. *Frontiers in Toxicology*, 4:881347, 2022. doi: 10.3389/ftox.2022.881347.